Applied Fault Detection and Diagnosis for Industrial Gas Turbine Systems

Yu Zhang[1] Chris Bingham*[1] Mike Garlick[2] Michael Gallimore[1]

[1] School of Engineering, University of Lincoln, Lincoln, LN6 7TS, U.K.

[2] Siemens Industrial Turbomachinery, Lincoln, LN6 3AD, U.K.

Abstract: The paper presents readily implementable approaches for fault detection and diagnosis (FDD) based on measurements from multiple sensor groups, for industrial systems. Specifically, the use of hierarchical clustering (HC) and self-organizing map neural networks (SOMNNs) are shown to provide robust and user-friendly tools for application to industrial gas turbine (IGT) systems. HC fingerprints are found for normal operation, and FDD is achieved by monitoring cluster changes occurring in the resulting dendrograms. Similarly, fingerprints of operational behaviour are also obtained using SOMNN based classification maps (CMs) that are initially determined during normal operation, and FDD is performed by detecting changes in their CMs. The proposed methods are shown to be capable of FDD from a large group of sensors that measure a variety of physical quantities. A key feature of the paper is the development of techniques to accommodate transient system operation, which can often lead to false-alarms being triggered when using traditional techniques if the monitoring algorithms are not first desensitized. Case studies showing the efficacy of the techniques for detecting sensor faults, bearing tilt pad wear and early stage pre-chamber burnout, are included. The presented techniques are now being applied operationally and monitoring IGTs in various regions of the world.

Keywords: Fault detection and diagnosis, hierarchical clustering, self-organizing map neural network.

1 Introduction

The purpose of fault detection is to automatically generate an ‘alarm’ or ‘flag’ to inform operators of impending or developing failure, whilst fault diagnosis aims to identify the location and predict the consequences of the failure [1]. The adoption of ‘early warning’ systems to identify and localize emerging faults has therefore attracted considerable attention due to the widely-recognized benefits of facilitating reduced down-time and assurance of safety, through the use of fault detection and diagnosis (FDD)[2,3] algorithms.

Of the methods previously explored to date, FDD techniques can be broadly divided into three categories viz. knowledge-, model- and signal processing-based approaches [3,4,5]. Knowledge- based approaches often rely on monitoring residuals between multiple sensor measurements [6], however, due to the high number of sensors used on modern industrial gas turbines (IGTs) and other complex industrial systems, the adoption of additional redundant sensors is prohibitively expensive. When using model-based approaches, a virtual sensor (a ‘model’ by some description) is employed to provide an estimate of expected measurements, from which residuals are then used as an indicator of potential failure modes being present [3]. However, for large IGT systems, which are often custom-designed to meet individual orders, the use of application specific materials and components (for example, to satisfy off-shore oil platform regulations) often makes the identification of an accurate dynamic model that can accommodate the full operating envelope, extremely difficult. In such circumstances, techniques based on direct signal processing and data fusion provide more practical and efficient FDD solutions [4].

Considering signal processing-based FDD

Manuscript received date; revised date
* Corresponding author:
Tel: +44 1522 837912; Email:cbingham@lincoln.ac.uk

approaches, principal component analysis (PCA) [7] and artificial neural networks (ANNs) [8] have been the most popular candidate solutions to date. PCA based squared prediction error (SPE) is well established and extensively applied to detect sensor faults in industrial processes and power control [9,10,11]. However, since SPE alone cannot identify the faulted sensor, additional algorithms are applied for sensor fault identification. For instance, sensor validity indices (SVIs) are introduced in [10], and graphical SPE-contribution plots are presented as a supplement to SPE to identify the sensor or component at fault in [11]. Moreover, for FDD, candidate ANN techniques are mainly based on multi-layer perceptron neural networks (MLPNNs) [12] and self-organizing map neural networks (SOMNNs) [13]. Outputs from MLPNNs, in particular, have been compared with the performance from support vector machine (SVM) based techniques [14,15] for FDD in rotating machinery. Specially, in [16], ANNs are used with pre-processed vibration signals as input features. Although the SVM solution presented in [16] cannot be considered optimal in the cited instance, the authors nevertheless concluded that ANNs achieved a high performance success rate compared to solutions from SVMs, and that ANNs are more readily trained (with regard to required computation overhead) and more robust than SVMs. SOMNNs have also demonstrated good performance for FDD in induction machines [17], with [18] concluding that SOMNNs generally provide better solutions than MLPNNs and other radial basis function neural networks (RBFNNs) for this application field.

Considering cluster analysis methodologies, some precedence also exists for their use in FDD. Compared to the use of 'black-box' models typical of those used in ANNs, and alternative complex eigenvector-eigenvalue techniques of PCA, cluster analysis is a more straightforward technique derived from relatively basic distance algorithms, and have therefore gained favour since they are readily implemented and interpreted. Specifically in [19], four unsupervised clustering models are employed, including SOMNNs, hierarchical tree models and quality adaptive threshold models, along with a new hybrid model for FDD of industrial robots. From the results, the authors conclude that supervised classification algorithms often fail when encountering new data, whilst in contrast, unsupervised techniques, such as SOMNNs and hierarchical clustering (HC) methods, are more robust for novelty detection [19,20]. The authors of [21] applied HC to monitor a large group of sensors for the wide area backup protection of electric power systems. They conclude that HC could accomplish FDD successfully, and the dendrograms of HC provided an intuitive presentation mechanism.

In this paper, HC and SOMNN are applied for FDD to provide a corroborative early warning system. Whilst typically, fault diagnosis algorithms are applied after the initial detection of an emerging fault, thereby forming a two-stage FDD procedure [1,2], here, the proposed FDD approaches both detect and identify emerging faults in a single stage. Another key aspect of this paper is an investigation of how the techniques can accommodate transient operational conditions that typically generate unexpected 'false alarms' resulting in unnecessary unit shutdowns. This often occurs as a consequence of algorithms being 'tuned' during steady operational conditions, for instance [22,23], and are typically addressed by subsequently desensitizing the monitoring algorithms, which then leads to the non-detection of genuine fault conditions.

2 Problem Statement

In this paper, two large groups of sensors on an IGT system are used to focus the study. The IGT consists of 3 stages viz. compressor (gas turbine), combustion chamber and power turbine, as shown in Fig. 1, and are classified according to the amount of power they generate and their functionality.

A group of 19 sensors, labelled 'Group 1', includes 13 engine exhaust gas temperature (EGT) sensors (sensors EGT1 to 13) and 6 pilot burner-tip temperature (BTT) sensors (sensors BTT1 to 6). Additionally, a second group, Group 2, consists of a

set of 16 sensors

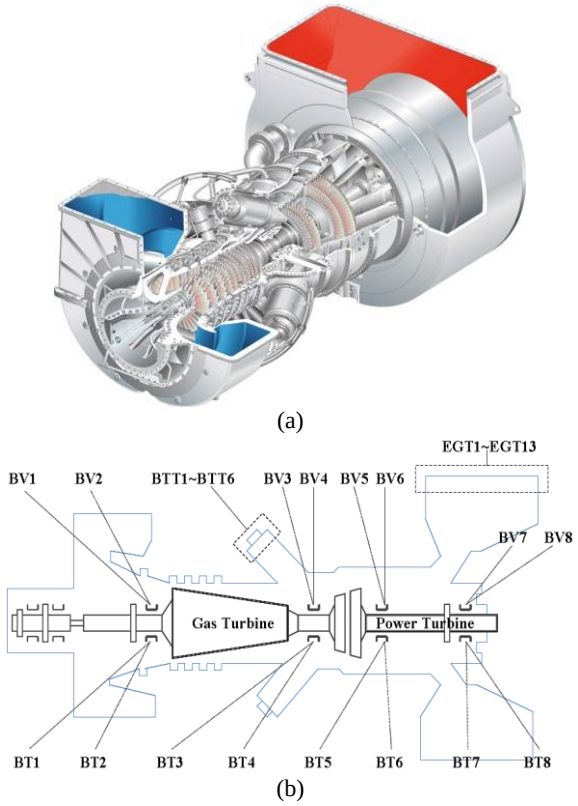

(a)

(b)

Figure 1. (a) Schematic of an industrial gas turbine system; (b) Sensor positioning: Group 1 -- EGT and BTT sensors, and Group 2 -- BV and BT sensors

that provide 8 bearing vibration (BV) measurements (sensors BV1 to 8) and 8 bearing temperature (BT) sensors (sensors BT1 to 8), that are sited orthogonally on the turbine units (Fig. 1(a)), as indicated in simplified form in Fig.1(b).

Here, HC and SOMNN solutions are developed for FDD on the IGTs. Through HC, operational 'fingerprints' are constructed from daily HC dendrograms which are then compared with dendrograms that are considered to represent 'normal operation' of the unit, in order to detect and identify faults. In this instance, the data sampling rate is one sensor set measurement per minute. Similarly, through the use of SOMNNs, which can also provide a visual classification of data suitable for operator interpretation as well as numerical outputs, the resulting classification maps (CMs) are compared with the normal 'fingerprint' CMs, to provide additional corroborating evidence to support the detection results from HC. The efficacy of the developed techniques is demonstrated through the use of three case studies to detect i) burner-tip pre-chamber burnout caused by contamination in the gas fuel system, ii) sensor fault as a consequence of low supply voltage, and iii) detection of tilt pad fretting caused due to absence of lubricant. Early detection of these types of emerging faults and the identification of affected components prevent unnecessary consequential damage to the engine and subsequent downtime. The information also facilitates flexible maintenance scheduling as opposed to a calendar-based approach which is typical of the sector.

3 Underpinning Concepts

3.1 Hierarchical clustering

The underlying concept of agglomerative HC is to assemble a set of objects into a hierarchical tree, where similar objects join in lower branches and these branches further join based on object 'similarity'. Objects with the smallest 'distance' between them are joined by a branch of a tree (i.e. a cluster). Further clusters are then formed from merged sub-clusters, and the hierarchical process iterates until only one cluster remains. The resulting hierarchical tree is then dissected according to either the linkage-distance or cluster number, and in so doing is used to provide novelty detection.

To facilitate clustering of the sensor data, one of many traditional 'distance functions' that have been previously reported could have been adopted. However, for simplicity, the most common measure is used here, the Euclidean distance:

$$d(\boldsymbol{x},\boldsymbol{y}) = \sqrt{\sum_{i=1}^{N}(x_i - y_i)^2} \quad , \tag{1}$$

where $\boldsymbol{x}$ and $\boldsymbol{y}$ are two $1\times N$ vectors, i.e. the signals, $(x_1, x_2, ..., x_N)$ and $(y_1, y_2, ..., y_N)$. A cluster is formed when the data from two sensors in a group have the minimum Euclidean distance—for instance, sensors EGT5 and EGT7 in Fig. 2. The first iteration provides the lowest ranking cluster. The procedure is subsequently iterated, including already constructed

clusters, to link higher ranking clusters (see [24] for an account of the underlying procedure).

An average linkage measure is used to calculate the mean distance between all pairs of objects in clusters *m* and *n*:

$$D(m,n)=\frac{1}{N_m N_n}\sum_{j=1}^{N_m}\sum_{k=1}^{N_n} d\left(\boldsymbol{x}_{mj},\boldsymbol{y}_{nk}\right). \qquad (2)$$

where $j=1,2,...,N_m$ and $k=1,2,...,N_n$. $d\left(\boldsymbol{x}_{mj},\boldsymbol{y}_{nk}\right)$ is the distance between two objects in the two clusters. N_m is the number of objects in cluster *m*, and N_n is the number of objects in cluster *n*. For instance, in Fig. 2, the distance between the EGT sensor branch and the BTT sensor branch is calculated by the average sum of the distances of all the sensors between these two branches, where $N_m=13$ and $N_n=6$.

In this way, a visual representation of the correlation between sensed variables, and between measurements from multiple sensors, can be readily used as a 'fingerprint' of unit operational characteristics. By comparing such fingerprints with those derived from subsequent batch measurement sets taken on a daily basis, the emergence of 'novelty' in the unit's operation can be identified prior to catastrophic failure. For the application considered here, an example 'normal' fingerprint for 'Group 1' sensors is shown in Fig. 2, which is generated from the sample temperature measurements in Fig. 3. It can be seen that a clear separation exists between the data from the EGT and the BTT sensors in the dendrogram, although it is less apparent from the raw measurement data.

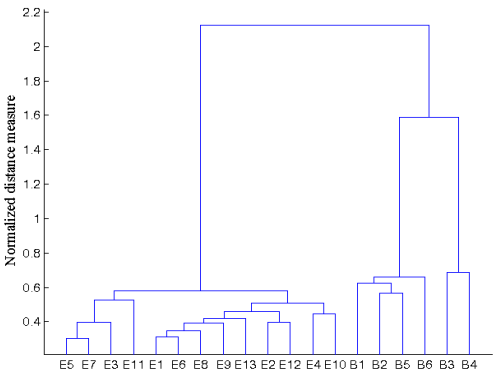

Figure 2. HC dendrogram: fingerprint for normal operation (Group 1: E=EGT; B=BTT)

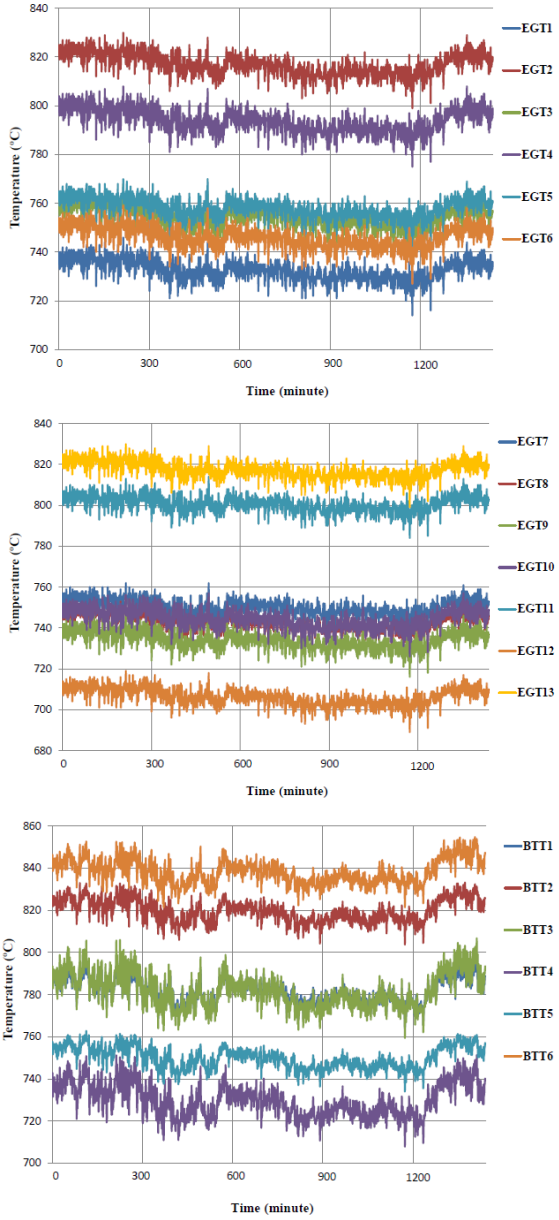

Figure 3. Temperature measurement taken during normal operation (Group 1): 13 EGT sensors; 6 BTT sensors

3.2 Self-organizing map neural networks

A SOMNN is a competitive ANN, using unsupervised learning to produce a discretized representation (typically in two-dimensions) of the input space, called a 'self-organizing map' (SOM) [25]. The input data vector, in this case a sampled sensor signal, $\boldsymbol{x}=\left[x_1,x_2,...,x_N\right]\in\Re^N$, with *N* variables, is associated with a reference vector, $\boldsymbol{r_i}\in\Re^N$, which is often randomly initiated to give

each neuron a displacement vector in the input space. For each sample of $\boldsymbol{x}(t)$, $\boldsymbol{r}_w(t)$ constitutes 'the winner', by seeking the minimum distance between the input vector and the reference vector, and is calculated from:

$$\|\boldsymbol{x}(t)-\boldsymbol{r}_w(t)\| \le \|\boldsymbol{x}(t)-\boldsymbol{r}_i(t)\| \quad \text{for} \quad \forall\, i\,. \tag{3}$$

After obtaining a 'winner', the reference vectors are updated using:

$$\boldsymbol{r}_i(t+1) = \boldsymbol{r}_i(t) + n_{w,i}(t)\big(\boldsymbol{x}(t)-\boldsymbol{r}_i(t)\big), \tag{4}$$

where $n_{w,i}(t)$ is a neighbourhood function that is normally chosen to be Gaussian. The reference vectors are adjusted to match the training signals, in a regression process over a finite number of steps, in order to achieve the final SOMs.

For this specific application field, SOMNN training is performed initially using measurements considered to reflect 'normal operation', as shown in Fig. 3, with 19 variables and 1440 time samples in the network. To obtain a visual output of the classifications, the SOMNN is initially trained with the output space depicted as 8×8 hexagonal grids, using MATLAB Neural Network Toolbox [26]. Here, 1440 samples of the 19-dimensional (sensor measurement) data are projected into the 64 neurons (clusters), that form a map in a two-dimensional space topologically (see the 8×8 hexagonal grids shown in Fig. 4). Through training, the reference vector of each neuron moves closer to the cluster center according to the samples that are clustered in the neuron, and the neighboring neurons also move closer to one another, eventually forming the final SOM. The sample hits i.e. how many samples (out of the 1440 samples) are clustered into each neuron, are shown in Fig. 4. For instance, for the (circled) top left node, 8 samples from the original input are clustered into this neuron.

After being clustered, the weight vectors of the 64 neurons are calculated for each variable independently, by comparing the variable (signal) with the reference vectors of the neurons (the cluster centers after training) in the final SOM. In this way, 19 component (variable) weighting planes (matrices) are calculated, as shown in Fig. 5, with each subplot considered as a visualization of the weights from the variable (input) to the neurons (output), which can be considered as the deviations of each measurement from the 19 sensors' average characteristic. A dark color on a particular grid indicates a stronger connection between the input and the output, and vice-versa. The component weight planes provide convenient visual interpretations since connection patterns that are similar mean that the variables are highly correlated, and vice-versa. From the results in Fig. 5, for instance, a clear separation of the weighting matrices is evident between EGT1—EGT13 and BTT1—BTT6 during normal operation. This is therefore again considered as a 'fingerprint' of the unit's behaviour whilst operating normally. It is a comparison of fingerprints from subsequent measurements, and the changes that are identified, that are considered to provide FDD.

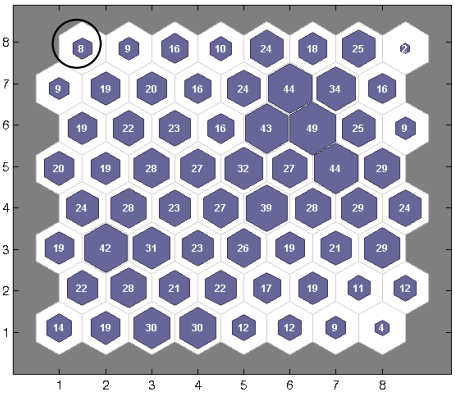

Figure 4. SOMNN neuron sample hits from 1440 samples of data from the 19 sensors

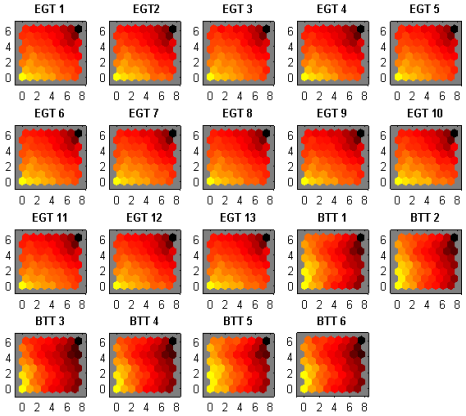

Figure 5. Component planes of the map for normal operation (Group 1)

4 Application Case Studies

For remotely monitored GT units, a HC tree (dendrogram) is automatically generated using daily batched measurement processing, which is then compared with the normal operation HC fingerprint (Fig. 2) for FDD. Similarly, the SOMNN is applied to data from the unit on a real-time basis to detect deviations from normal behaviour i.e. novelty detection, through the use of SOM component planes and classification maps (CMs). The application of HC and SOMNN for FDD in this manner is now presented with results taken from three example case studies.

4.1 Case 1: detection of pre-chamber burnout

By comparing batch measurement data taken on a daily basis with the 'normal' HC fingerprint in Fig. 2, faults can be detected by identifying cluster changes in the dendrograms. By way of example, Fig. 6 shows a subsequently developed dendrogram that does not 'fit' the normal fingerprint in Fig. 2. In this case, sensor BTT6 resides in a higher sub-cluster, where the normal fingerprint shows the EGT and the BTT sensors in two main clusters that are equally separated. This is indicative of a change in characteristics. By consulting the actual sensor measurements in Fig. 7, it is clear that a fault relating to measurements from BTT6 is evidently emerging.

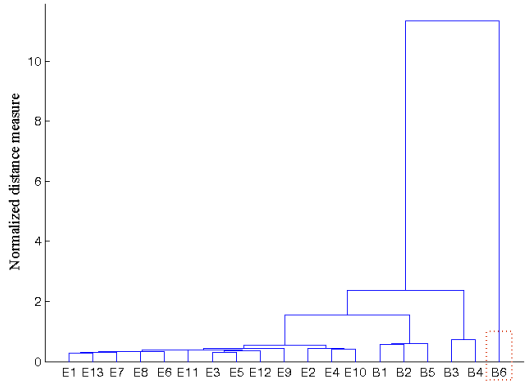

Figure 6. Case 1: HC dendrogram indicating sensor BTT6 anomaly (E=EGT; B=BTT)

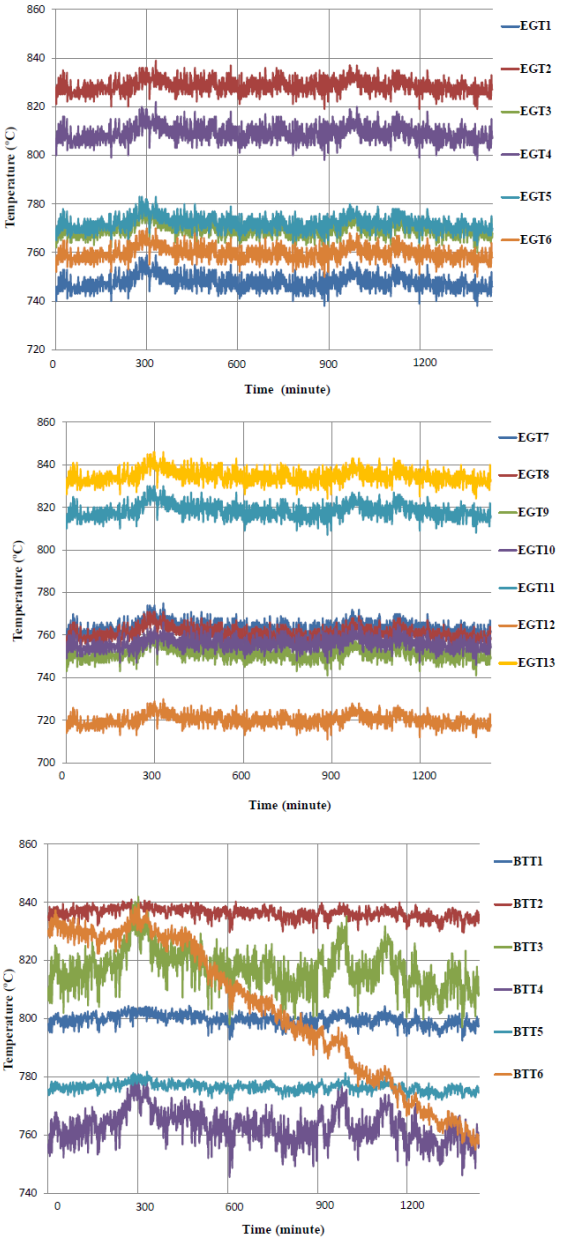

Figure 7. Case 1: Temperature measurements showing an emerging fault relating to sensor BTT6.

Notably, the measurements remain within the normal range and would not have been flagged as evidence of an emerging fault to an operator at this relatively early stage. The HC has therefore provided an early warning of a developing abnormal situation.

Similarly, the measurements in Fig. 7 are also applied to the SOMNN resulting in the calculated component planes shown in Fig. 8. If the weighting planes are considered as a contour map of a 3-D surface, where the color, from light to dark, indicates, respectively a range from minimum to maximum, it can be seen that the 'surface' corresponding to sensor

BTT6 is characterized by principal directions and curvatures that are notably different from those of the other sensors. In this way, it is clear that a distinction between the expected and real behaviour of BTT6 has been identified. Crucially, this is also commensurate with the results of HC.

Although the graphical interpretation is convenient for trained operators, to provide an automated 'alarm' an alternative numerical interpretation can also be obtained by applying the SOMNN to give a 2-classification output. The resulting abnormal classification map data (ACM) is given in Table 1, where sensor BTT6 is clustered into class 2 rather than into class 1 as would be expected by comparing to the normal classification map (NCM) – refer to the clustering in Fig. 6 to see the exact correspondence. As well as being consistent with the results from the component planes (Fig. 8) and thereby indicating 'abnormal characteristics', it also readily provides for a simple 'early warning flag' for the operator.

In this instance, subsequent field investigations identified a BTT6 measurement outlier due to the presence of liquid hydrocarbon based contamination within the gas fuel system. The hydrocarbon based contaminant is introduced into the combustion system as a 'slug' that impinges onto the wall of the flame tube pre-chamber causing localised temperature changes—see Fig. 9. The BTT6 measurement is seen to be significantly lower in temperature over time following the pre-chamber burnout which is caused by the extra air being introduced via the pre-chamber of the flame tube. In this instance, the BTT measurement gradually diverged by ~300ºC resulting in incomplete combustion and increased levels of emissions from the IGT. Typically, BTTs are monitored within lean pre-mixed Dry Low Emission combustion systems and protect the turbine by using temperature limits to shutdown the unit if they are exceeded. However, in this case, combustion damage occurs without reaching these limits.

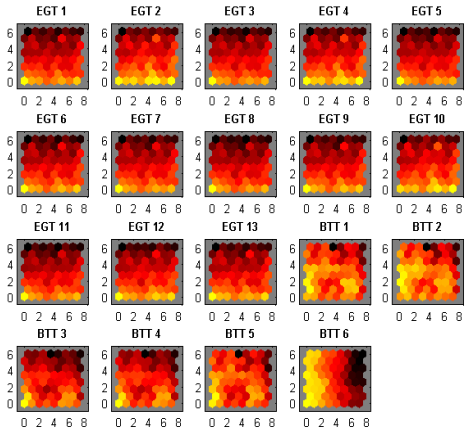

Figure 8. Case 1: Component planes of the map showing BTT6 fault

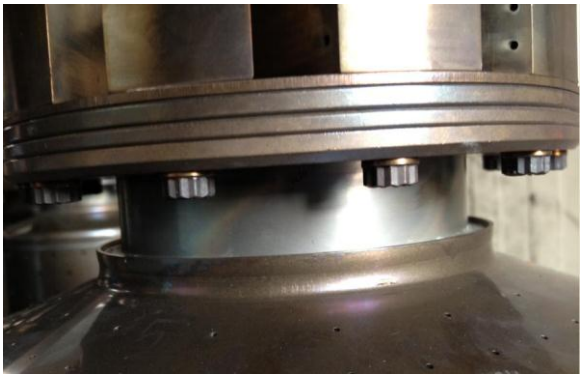

(a)

(b)

Figure 9. Photos of (a) an early stage of pre-chamber burnout; (b) a pre-chamber burnout failure

4.2 Case 2: detection of sensor fault

Fig. 10 shows example 'Group 2' measurement data when the system is considered to be operating normally. Using the HC approach, a 'normal operational fingerprint' of the unit is determined, as shown in Fig. 11.

By deriving HC dendrograms using subsequent daily batches of data, an alternative dendrogram was detected at a later date—see Fig. 12. In this case, Fig. 12 identifies 'novelty' from the measured data from sensor BV6, as a result of a change in its associated

cluster grouping. By subsequently consulting the raw data (Fig. 13), the fault is clearly evident.

Notably, by using simple classical detection limits to identify anomalies, the fault would not have been captured. However, by inherently incorporating the interrelationship between groups of sensor measurements, the HC recognizes the 'novel' characteristic.

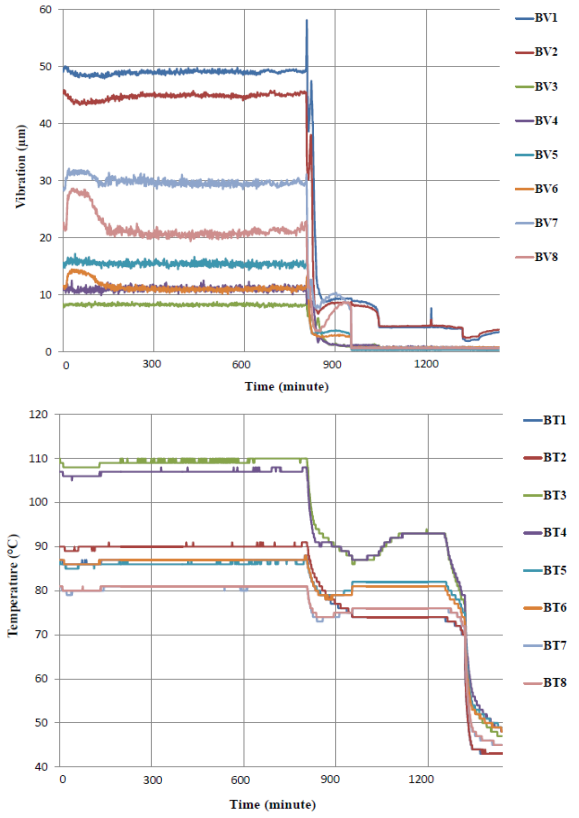

Figure 10. Measurements during normal operation (Group 2): 8 BV sensors; 8 BT sensors.

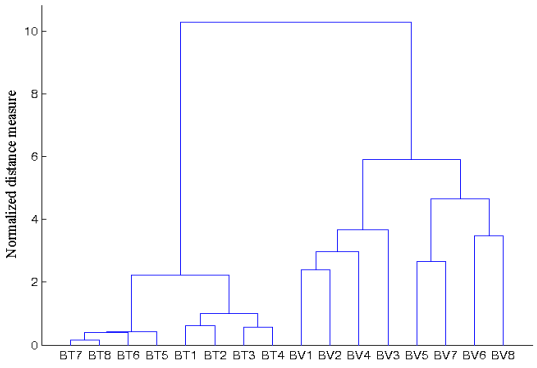

Figure 11. HC dendrogram: fingerprint for normal operation (Group 2)

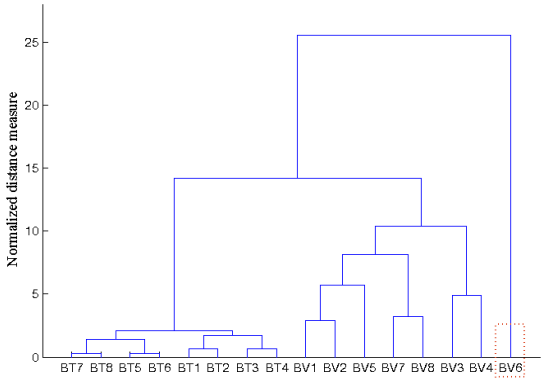

Figure 12. Case 2: HC dendrogram showing sensor BV6 anomaly

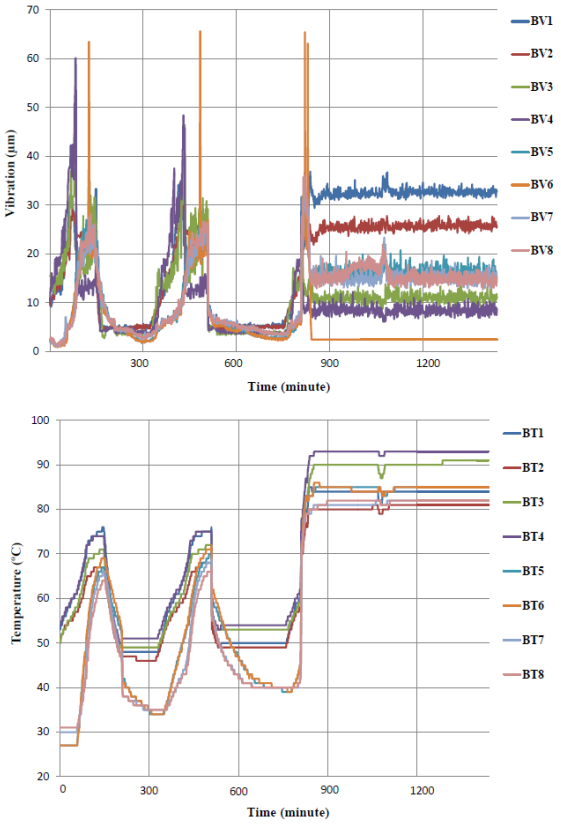

Figure 13. Case 2: Vibration and temperature information indicating a fault in BV6 sensor.

To provide corroborating evidence, a SOMNN is also trained using the measurements shown in Fig. 10, with 16 variables (BV1—BV8 and BT1—BT8) in the network. The weighting matrices of 64 neurons for the 16 sensors are shown in Fig. 14, which is given to provide a separation between BV1—BV8 and BT1—BT8 during normal operation (matching the HC results in Fig. 11). The component planes of the subsequent maps derived from the measurements

in Fig. 13, are shown in Fig. 15, which, once again identifies that sensor BV6 is providing different characteristics compared to the other sensors (consistent with the HC outputs in Fig. 12).

To aid in the generation of automatic alerts, the SOMNN is also trained to classify the data from the 16 sensors into 2 patterns (with indices 1 and 2), with the NCM and the ACM in this case being shown in Table 2, where the NCM shows two classifications between the BV and the BT sensors, and the ACM shows that sensor BV6 is classified as an abnormal sensor measurement set in the group.

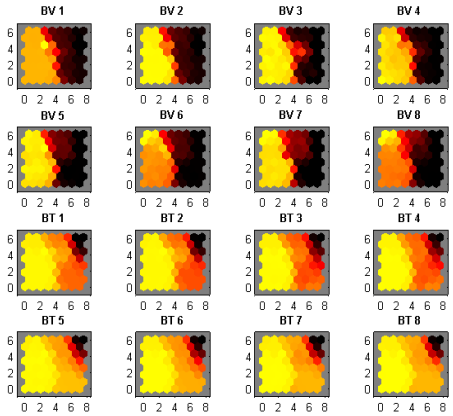

Figure 14. Component planes of the map for normal operation (Group 2)

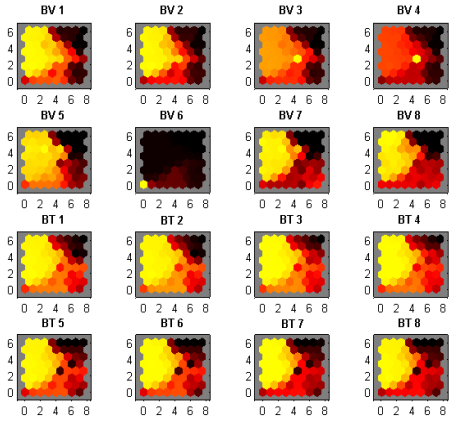

Figure 15. Case 2: Component planes of the map showing BV6 sensor fault

In this case, subsequent field investigations showed a trend of transient spikes on measurements from BV6, followed by long periods of constant steady readings over protracted durations caused by transient short circuits and subsequent low-battery voltages that power the sensor. In this case, after FDD, the faulted sensor was replaced for assurance of safety and reliability, but without needing to shut down gas turbine unit—and thereby facilitated greater unit availability.

4.3 Case 3: detection of bearing fault

The proposed HC and SOMNN approaches are readily applicable to the identification of component faults that become evident from anomalous measurements from sensors clusters and/or sensors from different groups. By way of example, Fig. 16 shows batch vibration and temperature data that has been applied to the HC and SOMNN algorithms. The resultant HC dendrogram is shown in Fig. 17. It can be seen that both BV1 and BV2 are clustered outside their ‘normal’ fingerprint. Since BV1 and BV2 sensors are sited at adjacent locations on the gas turbine inlet bearing, this is indicative of a machine component fault at that location (as opposed to multiple sensor faults).

Similarly from the SOMNN, the resultant component planes, after training, are shown in Fig. 18 (corroborating the results from HC in Fig. 17), and by comparison with the NCM, the 2-classification results (ACM) in Table 3, show that both BV1 and BV2 indicate different characteristics from that expected from other sensor measurements, again indicating the emergence of a localized component fault.

Subsequent investigations focused on the identified inlet bearing, shown in Fig. 19(a), which has a diameter of ~150mm and runs at speeds in excess of 14,000rpm, and is subject to radial loads upto 3.0kN, and thrust loads upto 30kN. The tilt pads are ~10mm thick and ~42mm in length, as shown in Fig. 19(b). The bearing failure in this instance is caused by wear on the back of the tilt pad by fretting, with the bearing and the failed tilt pad shown in Fig. 20(a) and (b), respectively. By comparison with unworn bearings, Fig. 19, the metal damage of the tilt pad (localized wear) in Fig. 20 is clearly evident. This is caused by metal-to-metal material incompatibility due to the absence of lubricant at the contact areas between the bearing assembly and the tilt pad, so that

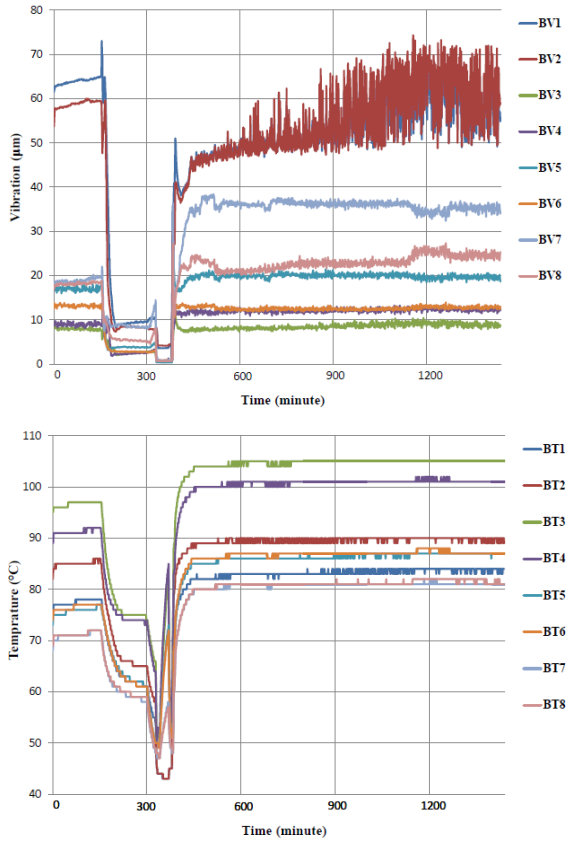

Figure 16. Case 3: Vibration and temperature measurements indicating a bearing fault from BV1 and BV2.

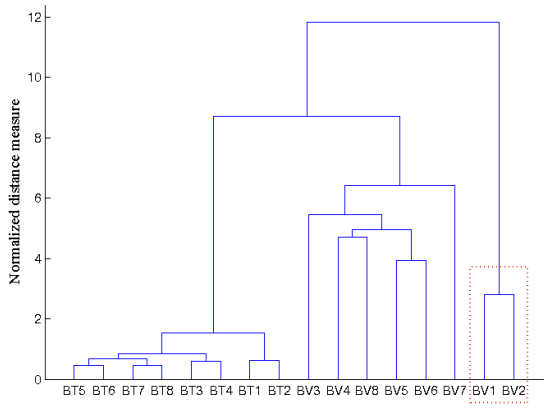

Figure 17. Case 3: Dendrogram indicating gas turbine inlet vibration bearing (BV1 and BV2) fault.

eventually the tilt pad does not tilt anymore, resulting in final bearing failure.

Although the presented HC technique is demonstrated to be of significant benefit for FDD, no direct 'error estimation' mechanism to monitor the efficacy of the algorithm is directly available. In such circumstances, it is therefore prudent to also use an alternative method for classification to provide corroborating evidence of emerging failures. A candidate unsupervised technique adopted here uses a SOMNN, which can again provide a visual classification of data suitable for operator interpretation, as well as provide numerical outputs for producing automated alerts. In this case, the resulting CMs are used to provide additional corrobo-

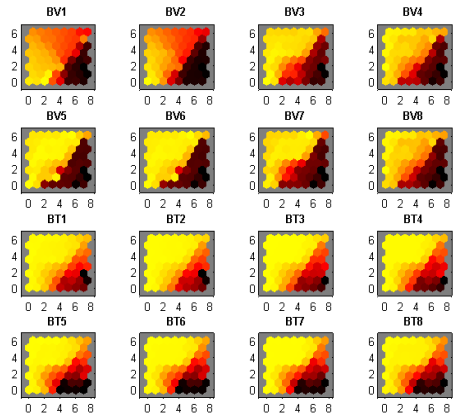

Figure 18. Case 3: Component planes of the map showing gas turbine inlet bearing fault (BV1 and BV2)

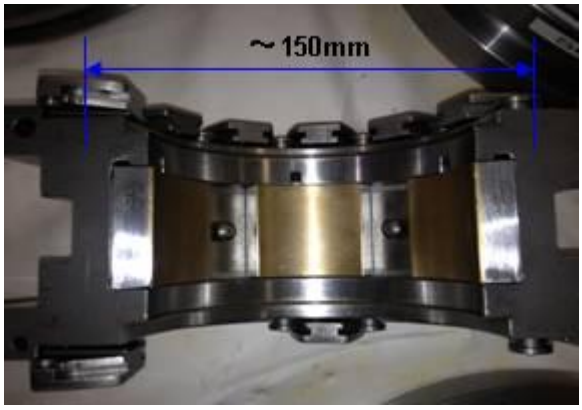

(a)

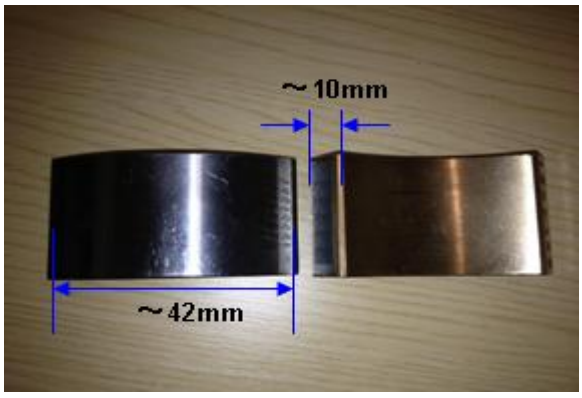

(b)

Figure 19. Photos of (a) a normal bearing (half assembly); and (b) the back and inside of normal tilt pads.

Table 1 Classification Maps (Case 1)

Sensors	$_{EGT}1$	$_{EGT}2$	$_{EGT}3$	$_{EGT}4$	$_{EGT}5$	$_{EGT}6$	$_{EGT}7$	$_{EGT}8$	$_{EGT}9$	$_{EGT}10$	$_{EGT}11$	$_{EGT}12$	$_{EGT}13$	$_{BTT}1$	$_{BTT}2$	$_{BTT}3$	$_{BTT}4$	$_{BTT}5$	$_{BTT}6$
NCM	1	1	1	1	1	1	1	1	1	1	1	1	1	2	2	2	2	2	2
ACM	1	1	1	1	1	1	1	1	1	1	1	1	1	1	1	1	1	1	2

Table 2 Classification Maps (Case 2)

Sensors	$_{BT}1$	$_{BT}2$	$_{BT}3$	$_{BT}4$	$_{BT}5$	$_{BT}6$	$_{BT}7$	$_{BT}8$	$_{BV}1$	$_{BV}2$	$_{BV}3$	$_{BV}4$	$_{BV}5$	$_{BV}6$	$_{BV}7$	$_{BV}8$
NCM	1	1	1	1	1	1	1	1	2	2	2	2	2	2	2	2
ACM	1	1	1	1	1	1	1	1	1	1	1	1	1	2	1	1

Table 3 Classification Maps (Case 3)

Sensors	$_{BT}1$	$_{BT}2$	$_{BT}3$	$_{BT}4$	$_{BT}5$	$_{BT}6$	$_{BT}7$	$_{BT}8$	$_{BV}1$	$_{BV}2$	$_{BV}3$	$_{BV}4$	$_{BV}5$	$_{BV}6$	$_{BV}7$	$_{BV}8$
NCM	1	1	1	1	1	1	1	1	2	2	2	2	2	2	2	2
ACM	2	2	1	1	1	1	1	1	1	1	1	1	1	1	1	1

(a)

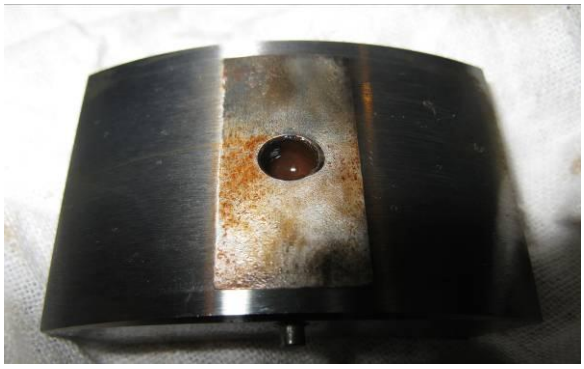

(b)

Figure 20. Photos of (a) a failed journal bearing; and (b) wear on the back of the tilt pad due to fretting.

rating evidence to support the detection results from HC dendrograms.

An advantage of using SOMNNs in this manner is that they can be simply realized with a numerical output. However, the 'black-box' nature of ANNs provides little insight into the relationship between the actual inputs and the ultimate confidence in the final results at the output. Nevertheless, the experimental trials do support their effectiveness as an 'early warning' of faults, and for facilitating an operator to subsequently discriminate which sensor or component is at fault.

A notable feature of the measurements in Fig. 10 for instance, is the data contains significant transients due to changes in load and power demand. Importantly, the HC 'fingerprint' is shown to be robust to such effects without creating undue false-alarms which is an unfortunate characteristic of other methods that often misclassify unless presented with steady-state data [22,23]. Conversely, even when masked by the effects of transient demand/load changes (Figs. 13, 16), abnormal characteristics due to faults are still correctly identified. As with the use of HC, the proposed SOMNN approach is also shown to accommodate operational transient behaviour without inducing false-alarms, whilst also correctly identifying failure modes—see Figs. 12, 17, and the resulting CMs in Tables 2, 3, for instance.

5 Conclusion

Both the HC and SOMNN approaches have been realised for automatic FDD. Daily datasets are downloaded from a fleet of IGTs, and are used to

provide daily reports of classification i.e. normal operation or abnormal operation, which include the identification of faulted sensor(s) and the location of emerging component failures. Although the techniques have been developed for, and applied to IGT systems here, ultimately the underlying principles are generic and are much more widely applicable to identifying fault modes in alternative complex systems with large sensor groups. The developed techniques are being used as part of a suite of agents that actively monitor IGTs across the various regions of the world.

Acknowledgments

The authors would like to thank Siemens Industrial Turbomachinery, Lincoln, U.K., for providing research support, access to on-line real-time data, and photos to support the research outcomes.

References

[1] M. Jiang, M. A. Munawar, T. Reidemeister, P. A. S. Ward. Efficient Fault Detection and Diagnosis in Complex Software Systems with Information-Theoretic Monitoring. *IEEE Transactions of Dependable and Secure Computing*, vol. 8, no. 4, pp. 510-522, 2011.

[2] Q. Y. Su, Y. C. Li, X. Z., Dai, J. Li. Fault Detection for a Class of Impulsive Switched Systems. *International Journal of Automation and Computing*, vol. 11, no. 2, pp. 223-230, 2014.

[3] F. Chen, S. Zhang, B. Jiang, G. Tao. Multiple Model-based Fault Detection and Diagnosis for Helicopter with Actuator Faults via Quantum Information Technique. *Proc. IMechE Part I: Journal of Systems and Control Engineering*, vol. 228, no. 3, pp. 182-190, 2014.

[4] A. Soualhi, G. Clerc, H. Razik. Detection and Diagnosis of faults in Induction Motor Using an Improved Artificial Ant Clustering Technique. *IEEE Transactions of Industrial Electronics*, vol. 60, no. 9, pp. 4053-4062, 2013.

[5] F. Lu, J. Huang, Y. Xing. Fault Diagnostics for Turbo-Shaft Engine Sensors Based on a Simplified On-Board Model. *Sensors*, vol. 12, no. 8, pp. 11061–11076, 2012.

[6] P. M. Frank. Fault Diagnosis in Dynamic Systems using Analytical and Knowledge-based Redundancy: A Survey and Some New Results. *Automatica*, vol. 26, no. 3, pp. 459-474, 1990.

[7] Y. Zhang, C. M. Bingham, M. Gallimore. Fault Detection and Diagnosis Based on Extensions of PCA. *Advances in Military Technology*, vol. 8, no. 2, pp. 27-41, 2013.

[8] W. Deng, X. Yang, J. Liu, H. Zhao, Z. Li, X. Yan. A Novel Fault Analysis and Diagnosis Method Based on Combining Computational Intelligence Methods. *Proc. IMechE Part E: Journal of Process Mechanical Engineering*, vol. 227, no. 3 , pp. 198-210, 2013.

[9] M.F. Harkat, S. Djelel, N. Doghmane, M. Benouaret. Sensor Fault Detection, Isolation and Reconstruction Using Nonlinear Principal Component Analysis. *International Journal of Automation and Computing*, vol. 4, no. 2, pp. 149-155, 2007.

[10] B. Lee, X. Wang. Fault Detection and Reconstruction for Micro-Satellite Power Subsystem Based on PCA. *Systems and Control in Aeronautics and Astronautics*, vol. 3, pp. 1169-1173. 2010.

[11] H. Liu, M.J. Kim, O.J. Kang, J.T. Kim, C.K. Yoo. Sensor Validation for Monitoring Indoor Air Quality in a Subway Station. *Sustainable Healthy Buildings*, vol. 5, pp. 477-489. 2011.

[12] Y. Li, M. J. Pont, N. B. Jones, J. A. Twiddle. Applying MLP and RBF Classifiers in Embedded Condition Monitoring and Fault Diagnosis Systems. *Transactions of the Institute of Measurement and Control*, vol. 23, no. 5, pp. 315-343, 2001.

[13] J. Yu. A Hybrid Feature Selection Scheme and Self-organizing Map Model for Machine Health Assessment. *Applied Soft Computing*, vol. 11, no. 5, pp. 4041-4054, 2011.

[14] X. Chen, T. Limchimchol. Monitoring Grinding Wheel Redress-life Using Support Vector Machines. *International Journal of Automation and Computing*, vol. 3, no. 1, pp. 56-62, 2006.

[15] N. Laouti, S. Othman, M. Alamir, N. Sheibat-Othman. Combination of Model-based Observer and Support Vector Machines for Fault Detection of Wind Turbines. *International Journal of Automation and Computing*, vol. 11, no. 3, pp. 274-287, 2014.

[16] L.B. Jack, A.K. Nandi. Fault Detection Using Support Vector Machine and Artificial Neural Networks Augmented by Genetic Algorithms. *Mechanical Systems and Signal Processing*, vol. 16, no. 2-3, pp. 373-390. 2002

[17] S. Wu, T.W. Chow. Induction Machine Fault Detection Using SOM-based RBF Neural Networks. *IEEE Transactions on Industrial Electronics*, vol. 51, no. 1, pp. 183-194. 2004.

[18] K. Elissa, L.F. Gonçalves, J.L. Bosa, T.R. Balen, M.S. Lubaszewski, E.L. Schneider, R.V. Henriques. Fault Detection, Diagosis and Prediction in Electrical Valves using Self-organizing Maps. *Journal of Electron Test*, vol. 10, pp. 1007-1020. 2011.

[19] A. Datta, C. Mavroidis, M. Hosek. A Role of Unsupervised Clustering for Intelligent Fault Diagnosis. *ASME International Mechanical Engineering Congress and Exposition*, USA. 2007.

[20] Y. Kun, W. Bao, Q. Hu, D. Yu. Abnormal Data Detection Based on Hierarchical Clustering. *Power Engineering*, vol. 25, no. 6, pp. 865-869. 2005.

[21] Y. Zhang, J. Zhang, J. Ma, Z. Wang. Fault Detection Based on Hierarchical Cluster Analysis in Wide Area Backup Protection System. *Energy and Power Engineering*, vol. 1, pp. 21-27. 2009.

[22] C. Romesis, K. Mathioudakis. Setting Up of a Probabilistic

Neural Network for Sensor Fault Detection Including Operation with Component Faults. *Journal of Engineering for Gas Turbines and Power*, vol. 125, no. 3, pp. 634-641. 2003.

[23] T. Kobayashi, D.L. Simon. Hybrid Kalman Filter Approach for Aircraft Engine In-flight Diagnostics: Sensor Fault Detection Case. *Journal of Engineering for Gas Turbines and Power*, vol. 129, no. 3, pp. 746-754. 2006.

[24] T. Hastie, R. Tibshirani, J. Friedman. 14.3.12 Hierarchical Clustering, The Elements of Statistical Learning (2nd ed.). New York: Springer. pp. 520–528. 2009.

[25] T. Kohonen. Self-organized Formation of Topologically Correct Feature Maps. *Biological Cybernetics*, vol. 43, pp. 59-69. 1982.

[26] MATLAB Version 7.10.0. Natick Massachusetts, the Mathworks Inc., 2010.

Yu Zhang received the B.Eng. degree from the School of Aerospace Engineering and Applied Mechanics, Tongji University, Shanghai, China, in 2004, and received the M.Sc. and Ph.D. degrees from the School of Civil Engineering, University of Nottingham, Nottingham, U.K., in 2005 and 2011, respectively. She is currently a Lecturer in the School of Engineering, University of Lincoln, Lincoln, U.K. Her research interests include fault detection and diagnosis, signal processing, neural networks and clustering analysis.

E-mail: yzhang@lincoln.ac.uk

Chris Bingham received the B.Eng. degree in Electronic Systems and Control Engineering, from Sheffield City Polytechnic, Sheffield, UK, in 1989, the M.Sc(Eng) degree in Control Systems Engineering from the University of Sheffield, Sheffield, UK, in 1990, and a Ph.D from Cranfield University, Swindon, UK, in 1994, where his research focused on control systems to accommodate nonlinear dynamic effects in aerospace flight-surface actuators. From 1994 to 2010, he held academic positions at the University of Sheffield as a Researcher, Lecturer and Senior Lecturer. He is currently Professor of Energy Conversion, and College of Science Director of Research at the University of Lincoln, Lincoln, UK. Prof. Bingham has made significant contributions to a diverse range of national and internationally funded research, with a bias towards industrial applications. He currently heads a research team investigating sensor fault detection and remedial strategies, and prognostic and diagnostic techniques for a global fleet of sub-15MW industrial gas turbines in order to maximize unit operational availability. He also actively pursues collaborative research into the modeling of the thermal environment of domestic buildings and their thermal control, and has a long-standing track record in EV/HEV research.

E-mail: cbingham@lincoln.ac.uk (Corresponding author)

Mike Garlick received the B.Eng. degree in Mechanical Engineering, from Sheffield Hallam University in 2013. Having worked at Siemens Industrial Turbomachinery Ltd (Lincoln) since 2005 with a background in Combustion design, he is currently working as a Service Support Engineer involved in Remote Monitoring projects.

E-mail: mike.garlick@siemens.com

Michael Gallimore received the B.Eng. degree in Mechanical and Computer Aided Engineering from Sheffield Hallam University, Sheffield, UK, in 2006. He is currently a Principal Lecturer in the School of Engineering, University of Lincoln, Lincoln, UK. Prior to this, he spent ten years working for Siemens Industrial Turbomachinery Ltd, Lincoln, UK with various roles including Design Engineer, Senior Support Engineer and Service Manager. His research interests include intelligent diagnostics and prognostics for complex systems, signal processing, optimization and biomedical engineering.

E-mail: mgallimore@lincoln.ac.uk